PHYSICAL REVIEW B **81**, 060507(R) (2010)

Unexpected Fermi-surface nesting in the pnictide parent compounds $BaFe_2As_2$ and $CaFe_2As_2$ revealed by angle-resolved photoemission spectroscopy

Takeshi Kondo,[1] R. M. Fernandes,[1] R. Khasanov,[2] Chang Liu,[1] A. D. Palczewski,[1] Ni Ni,[1] M. Shi,[3] A. Bostwick,[4] E. Rotenberg,[4] J. Schmalian,[1] S. L. Bud'ko,[1] P. C. Canfield,[1] and A. Kaminski[1]

[1]*Ames Laboratory and Department of Physics and Astronomy, Iowa State University, Ames, Iowa 50011, USA*

[2]*Laboratory for Muon Spin Spectroscopy, Paul Scherrer Institut, CH-5232 Villigen PSI, Switzerland*

[3]*Swiss Light Source, Paul Scherrer Institut, CH-5232 Villigen PSI, Switzerland*

[4]*Advanced Light Source, Berkeley National Laboratory, Berkeley, California 94720, USA*

(Received 3 May 2009; revised manuscript received 8 December 2009; published 19 February 2010)

We use angle-resolved photoemission spectroscopy to study the band structure of $BaFe_2As_2$ and $CaFe_2As_2$, two of the parent compounds of the iron arsenic high-temperature superconductors. Our high quality data reveals that although the Fermi surface is strongly three-dimensional, it does indeed have long parallel segments along the k_z direction that can lead to the emergence of magnetic order. More interestingly, we find very unusual incommensurate nesting of the Fermi surface in the *a-b* plane that is present only at low temperatures. We speculate that this is a signature of a failed charge density wave state that was predicted by renormalization-group studies.

DOI: 10.1103/PhysRevB.81.060507 PACS number(s): 74.70.−b, 74.25.Jb, 79.60.−i

The recent discovery of high-temperature superconductivity in iron arsenide based materials[1] has re-energized efforts to understand this fascinating phenomenon and renewed hopes of finding a new family of superconducting materials that would yield record high transition temperatures. As with the cuprates, the superconductivity in the iron arsenides occurs when an antiferromagnetic (AF) parent compound[2] is doped with carriers.[3,4] A notable difference between the two material classes lies in the ground-state properties of the parent compound. In the case of the cuprates it is insulating, whereas in the undoped iron arsenides it is metallic. The nature of the AF ordering in iron arsenide remains controversial; several studies attribute the magnetic ordering to an itinerant spin density wave (SDW),[5–7] while others favor magnetic order due to localized moments.[8] Another important distinction is that, unlike the cuprates, antiferromagnetism in the iron arsenides is thought to arise from strong nesting between hole and electron bands. If this is the case, the two-dimensional (2D) electronic properties are critical as they enhance the nesting conditions. Very recent reports demonstrate significant band dispersion along the k_z direction,[9,10] which implies a three-dimensional (3D) character of the electronic structure. It is therefore significant to understand if and how the strong nesting conditions are established and how the AF ordering affects the band dispersion and Fermi surface (FS). In order to address these issues, we performed angle-resolved photoemission spectroscopy (ARPES) on $BaFe_2As_2$ and $CaFe_2As_2$, two of the parent compounds for the iron arsenic high-temperature superconductors. We were able to identify a long straight segment of FS along the k_z direction that likely plays a significant role in the emergence of the magnetic order via strong $(\pi/a,\pi/a)$ nesting. We find strong in-plane band-back folding and corresponding hybridization effects that lead to a reconstruction of the FS below the magnetic ordering temperature (T_N). This gives rise to a characteristic "flowerlike" FS. These signatures of magnetic ordering are observed only along the k_z direction within a straight FS segment, which indicates a direct relation between good $(\pi/a,\pi/a)$ nesting and the emergence of AF ordering. More interestingly, we find long parallel segments of the Fermi surface within the *a-b* plane. The nesting vector is significantly shorter than the $(\pi/a,\pi/a)$ vector related to the magnetic order. We speculate that these nested parts of the Fermi surface may be a precursor of a failed CDW order predicted by renormalization-group studies.[11]

Single crystals of $BaFe_2As_2$ and $CaFe_2As_2$ were grown out of a FeAs flux as well as Sn flux using conventional high-temperature solution growth techniques.[12–14] $BaFe_2As_2$ and $CaFe_2As_2$ undergo a tetragonal to orthorhombic structural transition simultaneously with a paramagnetic to antiferromagnetic transition below $T_S \simeq T_N \simeq 130$ and 170 K, respectively.[13–16] ARPES data were measured at the SIS beamline of Swiss Light Source, Switzerland, the beamlines 7.0.1 of the Advanced Light Source (ALS), USA, using a Scienta R4000 analyzer and Ames Laboratory using a Scienta SES2002 with a Gammadata VUV5010 photon source. Energy and angular resolutions were 10–30 meV and ~0.1°, respectively.

Band calculations predict two types of nearly circular FS sheets in the paramagnetic state: a holelike FS centered at the zone center [Γ(Z)] and an electronlike FS centered at the zone corner (*X*).[17,18] Below the magnetic ordering temperature one would expect back folding and hybridization of these bands leading to a reconstruction of the FS.[18] Figures 1(a1) and 1(a2) show typical FS maps from a $BaFe_2As_2$ sample in the paramagnetic and magnetically ordered state, respectively. The FS does indeed display a more complicated structure in the magnetically ordered state than in the paramagnetic state. We show in Fig. 1(c2) a band dispersion map along a diagonal direction [blue arrow in Fig. 1(a2)]. In addition to the holelike bands that are characteristic of the paramagnetic state, we observe electronlike bands that are back folded from the *X* points about the antiferromagnetic zone boundary [AFZB, marked with red dashed lines in Fig. 1(a2)]. The presence of multiple Fermi crossings is evident in the multiple peaks in the momentum distribution curve (MDC) at the Fermi level in Fig. 1(c1). The two holelike bands and two electronlike bands can be also identified from

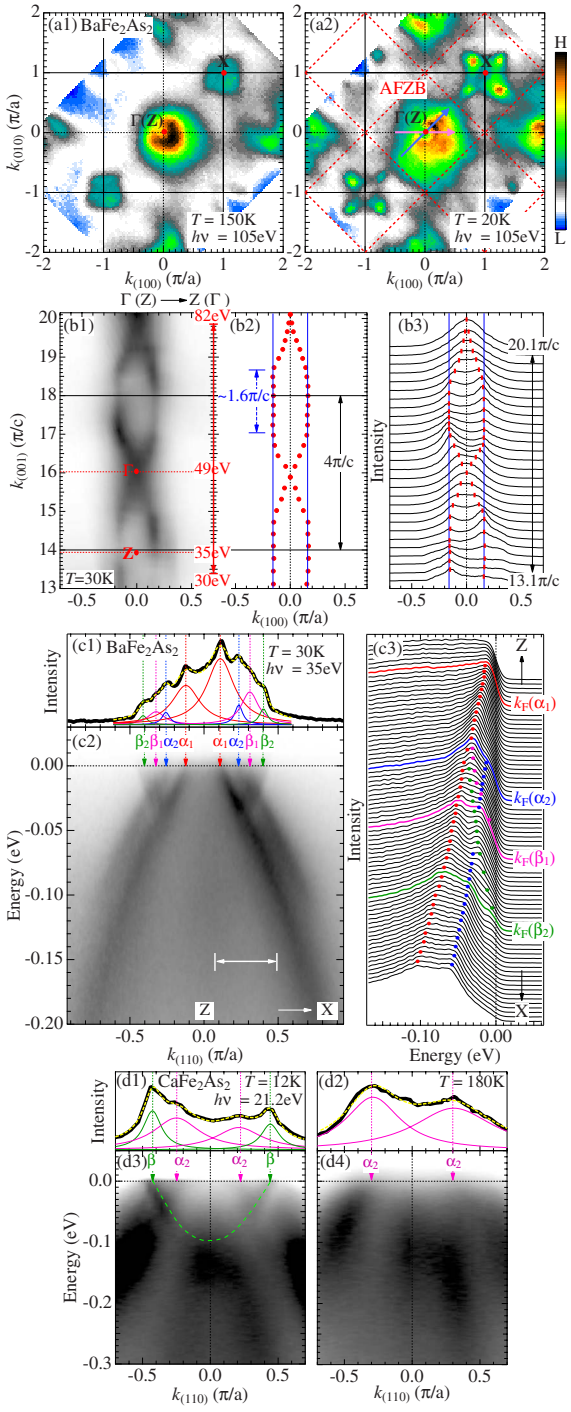

FIG. 1. (Color online) (a)–(c) $BaFe_2As_2$ and (d) $CaFe_2As_2$ data. FS map along a-b (a1) above and (a2) below T_N. (b1) FS map along $k_{(001)}$ and $k_{(100)}$ [horizontal pink arrow in (a2)]. (Inner potential: $V_0 \equiv 13$ eV) (b3) MDCs of (b1). (b2) FS plots of α_1 band extracted from peak positions of the MDCs. Blue dashed arrow indicates the parallel segment. (c1) MDC of (c2) at the Fermi energy and the fitting curve (yellow dashed curve). (c2) Band dispersion map along a diagonal cut [diagonal blue arrow in (a2)]. (c3) EDCs within a white arrow range in (c2). Circles follow hole bands (α_1 and α_2) and electron bands (β_1 and β_2). (d1)–(d2) MDCs at Fermi level of (d3)–(d4) and these fits (dashed yellow curves). Band dispersion map along a diagonal cut (d3) below and (d4) above T_N. Green dashed line is a guide to the eye for the electron band.

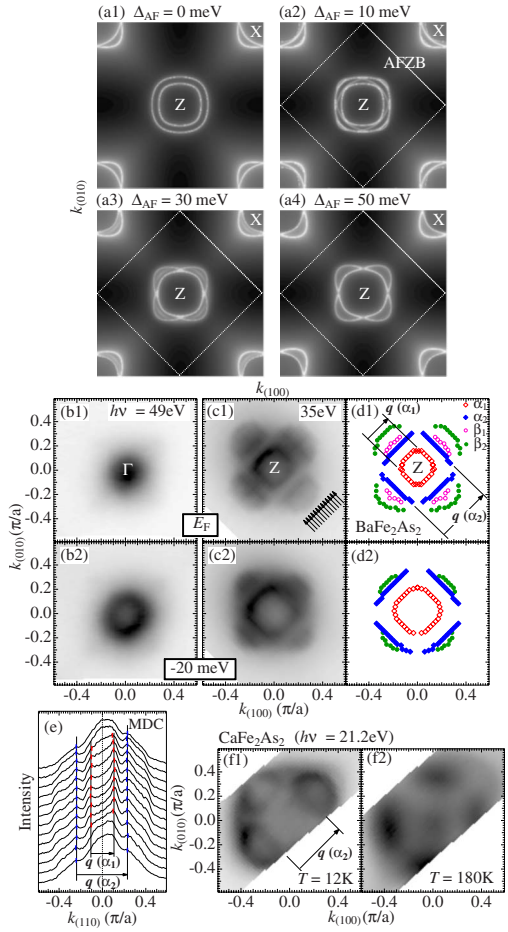

FIG. 2. (Color online) (a) Model calculation, (b)–(e) $BaFe_2As_2$, and (f) $CaFe_2As_2$ data. (a1) Model FSs in nonmagnetic phase. Reconstructed FSs for Δ_{AF} of (a2) 10, (a3) 30, and (a4) 50 meV. ARPES intensity about the Fermi energy and $E=-20$ meV obtained at (b1)–(b2) $h\nu=49$ eV (near Γ) and (c1)–(c2) $h\nu=35$ eV (near Z). (d1) FS and (d2) energy contour plots at $E=-20$ meV for $h\nu=35$ eV data. (e) MDCs along arrow directions in (c1). FS map close to the zone center along a-b plane (f1) below and (f2) above T_N. Dimension arrows indicate nesting vector $q(\alpha_1)=(0.16\pi/a, 0.16\pi/a)$ and $q(\alpha_2)=(0.33\pi/a, 0.33\pi/a)$ for hole band α_1 and α_2, respectively.

the peak positions of energy distribution curves (EDCs) as marked with color circles in Fig. 1(c3). In Figs. 2(c1)–2(d1), these bands hybridize leading to a reconstruction of the Fermi surface and the energy gaps (disconnected parts in the Fermi surface) with a consequent energy gain at the overlapped segments. We measured the ARPES data for $CaFe_2As_2$ below and above T_N. The Fermi-surface map near the zone center and the band dispersion map measured along a diagonal cut [blue arrow in Fig. 1(a2)] are plotted in Fig. 2(f1) and Fig. 1(d3) for below T_N and Fig. 2(f2) and Fig. 1(d4) for above T_N. The electron band (β, a dashed green guide line) is observed only below T_N [Fig. 1(d3)], and it is absent above T_N [Fig. 1(d4)]. The associated "flower-like" shape of Fermi surface changes to nearly circular as expected from band calculations in the nonmagnetic phase.

We demonstrate that a simple model with band-back folding about the AFZB incorporated reproduces many aspects

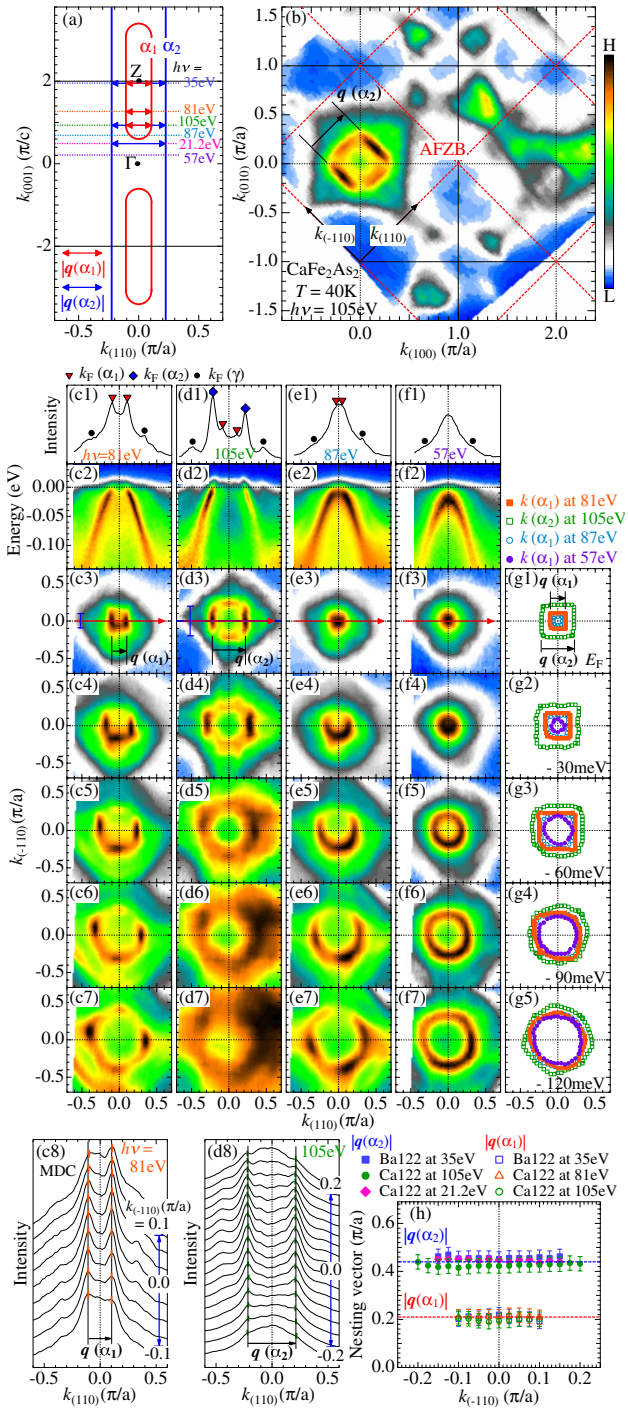

FIG. 3. (Color online) $CaFe_2As_2$ data below T_N. (a) Schematic FSs along $k_{(001)}$. (b) FS map along a-b plane. (c1)–(f1) MDC of (c2)–(f2) at the Fermi level. (c2)–(f2) Band dispersion map measured along a red arrow in (c3)–(f3). ARPES intensity about (c3)–(f3) Fermi level, (c4)–(f4) −30, (c5)–(f5) −60, (c6)–(f6) −90, and (c7)–(f7) −120 meV. (g1)–(g5) FS and energy contour plots extracted from (c)–(f). Only stronger peaks between $k_F(\alpha_1)$ and $k_F(\alpha_2)$ are plotted. Dimension arrows indicate a nesting vector $q(\alpha_1)=(0.15\pi/a,0.15\pi/a)$ and $q(\alpha_2)=(0.31\pi/a,0.31\pi/a)$ of hole band α_1 and α_2, respectively. (c8)–(d8) MDCs within a blue line indicators in (c3) and (d3). (h) $|q(\alpha_1)|$ and $|q(\alpha_2)|$ for $CaFe_2As_2$ (Ca122) and $BaFe_2As_2$ (Ba122) at various k_zs indicated with arrows in (a). [Inner potential: $V_0 \equiv 13$ eV for Ba122 and 20eV for Ca122]

of the data. Figure 2(a1) shows a model of two central hole- and corner electron pockets which is based on a band calculation for the nonmagnetic phase.[19] We assume that below T_N the states around Z are coupled to the states around X by an interband staggered mean field of magnitude Δ_{AF} via the mean-field term in the Hamiltonian $\Sigma_{\mathbf{k},\sigma}\sigma\Delta_{AF}(d^{\dagger}_{\mathbf{k},\sigma,\Gamma(Z)}d_{\mathbf{k}+\mathbf{Q},\sigma,X}+\text{H.c.})$, where σ refers to the spin and Q is the magnetic ordering vector. Upon increase of Δ_{AF} from 10 meV to 50 meV, the conduction bands are increasingly folded back about the AFZB and the Fermi surfaces are reconstructed in Figs. 2(a2)–2(a4) with twinning effects included.[20] The degree of the hybridization and reconstruction gets stronger with increasing Δ_{AF}. Eventually the FS becomes more "flowerlike." We plot the enlarged ARPES FS map of $BaFe_2As_2$ close to Γ and Z in Fig. 2(b1) and 2(c1), respectively, and the extracted Fermi crossing points for the latter in Fig. 2(d1). The experimentally observed "flowerlike" FS is well reproduced by the simple model for Δ_{AF} of 50 meV [Fig. 2(a4)]. Figure 2(b2) and 2(c2) shows the ARPES intensity close to Γ and Z, respectively, slightly below the Fermi energy ($E=-20$ meV). The band positions for the latter are plotted in Fig. 2(d2). While the effect of band hybridization ("flowerlike" shape) is clearly seen even in this energy range around Z [Fig. 2(c2)], it is absent around Γ [Fig. 2(b2)] with a round shape of the energy contour. The coupling between charge carriers and magnetism is therefore strongest whenever efficient low energy scattering between the two sets of FS is kinematically possible, demonstrating the role of interband magnetic scattering in the iron pnictides. Previous ARPES studies[9,10] demonstrated strong dispersion along the k_z direction. This raises a question about the origin of magnetic order and pairing, since the presence of strong k_z dispersion would significantly limit in-plane $(\pi/a,\pi/a)$ nesting. By acquiring high quality data [ARPES intensity map in Fig. 1(b1) and the corresponding MDCs in Fig. 1(b3)], we could see that, despite strong 3D-like dispersion, the Fermi surface has long $(\sim 1.6\pi/c)$ parallel segments along the k_z as seen in the extracted FS plots of Fig. 1(b2). The strong FS reconstruction discussed above is most prominent in this k_z range, which suggests that the parallel segments are significant for nesting conditions leading to the emergence of the $(\pi/a,\pi/a)$ magnetic order.

Perhaps the most interesting experimental observation in our data is an incommensurate FS nesting (long parallel segments of FS in the a-b plane seen in Fig. 2(d1) for $BaFe_2As_2$ and Fig. 2(f1) for $CaFe_2As_2$), which does not appear in the result of the model calculation [Fig. 2(a4)]. This is more clearly demonstrated in Fig. 2(e) using MDCs along the directions indicated in Fig. 2(c1) with arrows. The nesting vector $q(\alpha_1)\simeq(0.15\pi/a,0.15\pi/a)$ and $q(\alpha_2)\simeq(0.3\pi/a,0.3\pi/a)$ for hole band α_1 and α_2, respectively, does not correspond to any previously reported density wave states. Therefore, we speculate that the gapless, nested Fermi surface may be a precursor of a failed density wave order such as the CDW predicted by renormalization-group studies.[11] In order to investigate the k_z variation of the FS nesting, we measured FS maps along a-b for $CaFe_2As_2$ at various photon energies ($h\nu$). Figure 3(b) shows a typical FS map measured over a wide Brillouin zone with 105 eV photons. The reconstructed "flowerlike" FS and the significant

nesting with $q(\alpha_2) \simeq (0.3\pi/a, 0.3\pi/a)$ are clearly observed. In Fig. 3(c3)–3(f3), we plot the FS maps focused on the zone center ($\Gamma(Z)$) measured at various $h\nu$. The k_zs corresponding to these photon energies are indicated in Fig. 3(a) with the first Brillouin zone and schematic FS of hole bands (α_1 and α_2). We note that the intensity of several bands [α_1, α_2, and γ (Ref. 9)] dramatically changes with photon energy, and the electron bands (β_1 and β_2) are absent due to matrix element effects. These are confirmed in the MDCs at the Fermi level shown in Figs. 3(c1)–3(f1). In Figs. 3(c8) and 3(d8), we extract the FS from the MDC peak positions for regions marked with blue lines in panels Figs. 3(c3) and 3(d3), respectively. The FS nesting with $q(\alpha_1)$ and $q(\alpha_2)$ vectors is clearly seen. In panel (h) we plot the length of these vectors [$|q(\alpha_1)|$ and $|q(\alpha_2)|$] for $CaFe_2As_2$ and $BaFe_2As_2$ extracted from data at various k_zs shown in Figs. 2 and 3. The extracted portions of FS are schematically shown with arrows in
Fig. 3(a). The length of both vectors remains constant for a significant range of k_z momenta, indicating extensive nesting favorable for the formation of density waves. The presence of the α_2 nesting vector was recently confirmed by scanning tunneling spectroscopy experiments, where quasiparticle interference with a corresponding momentum value was clearly observed.[21] It is also worth noting that this nesting is identical in $CaFe_2As_2$ and $BaFe_2As_2$, which indicates that the nesting is universal for the parent compounds of the pnictides. We plot the energy contour intensities in (c4)–(f4), (c5)–(f5), and (c6)–(f6) ($E=-30$, -60, -90, and -120 meV, respectively). The parallel segments in the energy contours are significant up to $E \simeq -100$ meV. This binding energy seems to agree with the energy bottom of electron band back folded from the zone corner [see Fig. 1(d3)]. This indicates that the failed density wave order is tied to the existence of magnetic long-range order and suggests a strong coupling between the staggered magnetization and other density wave order parameters in the iron pnictides.

In conclusion, we find a relation between long parallel segments of Fermi surface along k_z and a reconstruction of the FS, which indicates that $(\pi/a, \pi/a)$ nesting is important for the magnetic ordering. More interestingly, we find long parallel segments of the Fermi surface in the *a*-*b* plane, which is not expected by the simple model. We speculate that these nested parts of the Fermi surface may be a precursor of a failed density wave order such as the CDW predicted by renormalization-group studies.[11]

We thank A. Kreyssig, A. I. Goldman, and B. N. Harmon for insightful discussions. ALS is operated by the U.S. DOE under Contract No. DE-AC03-76SF00098. Ames Laboratory was supported by the U.S. DOE, Basic Energy Sciences under Contract No. DE-AC02-07CH11358.

[1] Y. Kamihara, T. Watanabe, M. Hirano, and H. Hosono, J. Am. Chem. Soc. **130**, 3296 (2008).
[2] Clarina de la Cruz, Q. Huang, J. W. Lynn, Jiying Li, W. Ratcliff II, J. L. Zarestky, H. A. Mook, G. F. Chen, J. L. Luo, N. L. Wang, and Pengcheng Dai, Nature (London) **453**, 899 (2008).
[3] Jun Zhao, Q. Huang, Clarina de la Cruz, Shiliang Li, J. W. Lynn, Y. Chen, M. A. Green, G. F. Chen, G. Li, Z. Li, J. L. Luo, N. L. Wang, and Pengcheng Dai, Nature Mater. **7**, 953 (2008).
[4] H. Luetkens, H.-H. Klauss, M. Kraken, F. J. Litterst, T. Dellmann, R. Klingeler, C. Hess, R. Khasanov, A. Amato, C. Baines, M. Kosmala, O. J. Schumann, M. Braden, J. Hamann-Borrero, N. Leps, A. Kondrat, G. Behr, J. Werner, and B. Büchner, Nature Mater. **8**, 305 (2009).
[5] L. X. Yang, Y. Zhang, H. W. Ou, J. F. Zhao, D. W. Shen, B. Zhou, J. Wei, F. Chen, M. Xu, C. He, Y. Chen, Z. D. Wang, X. F. Wang, T. Wu, G. Wu, X. H. Chen, M. Arita, K. Shimada, M. Taniguchi, Z. Y. Lu, T. Xiang, and D. L. Feng, Phys. Rev. Lett. **102**, 107002 (2009).
[6] D. Hsieh *et al.*, arXiv:0812.2289 (unpublished).
[7] S. O. Diallo, V. P. Antropov, T. G. Perring, C. Broholm, J. J. Pulikkotil, N. Ni, S. L. Bud'ko, P. C. Canfield, A. Kreyssig, A. I. Goldman, and R. J. McQueeney, Phys. Rev. Lett. **102**, 187206 (2009).
[8] G. Liu, H. Liu, L. Zhao, W. Zhang, X. Jia, J. Meng, X. Dong, J. Zhang, G. F. Chen, Guiling Wang, Yong Zhou, Yong Zhu, Xiaoyang Wang, Zuyan Xu, Chuangtian Chen, and X. J. Zhou, Phys. Rev. B **80**, 134519 (2009).
[9] C. Liu, T. Kondo, N. Ni, A. D. Palczewski, A. Bostwick, G. D. Samolyuk, R. Khasanov, M. Shi, E. Rotenberg, S. L.Bud'ko, P. C.Canfield, and A. Kaminski, Phys. Rev. Lett. **102**, 167004 (2009).
[10] P. Vilmercati, A. Fedorov, I. Vobornik, U. Manju, G. Panaccione, A. Goldoni, A. S. Sefat, M. A. McGuire, B. C. Sales, R. Jin, D. Mandrus, D. J. Singh, and N. Mannella, Phys. Rev. B **79**, 220503(R) (2009).
[11] H. Zhai, F. Wang, and D.-H. Lee, Phys. Rev. B **80**, 064517 (2009).
[12] N. Ni, S. L. Bud'ko, A. Kreyssig, S. Nandi, G. E. Rustan, A. I. Goldman, S. Gupta, J. D. Corbett, A. Kracher, and P. C. Canfield, Phys. Rev. B **78**, 014507 (2008).
[13] N. Ni, S. Nandi, A. Kreyssig, A. I. Goldman, E. D. Mun, S. L. Bud'ko, and P. C. Canfield, Phys. Rev. B **78**, 014523 (2008).
[14] N. Ni, M. E. Tillman, J.-Q. Yan, A. Kracher, S. T. Hannahs, S. L. Bud'ko, and P. C. Canfield, Phys. Rev. B **78**, 214515 (2008).
[15] Marianne Rotter, Marcus Tegel, Dirk Johrendt, Inga Schellenberg, Wilfried Hermes, and Rainer Pöttgen, Phys. Rev. B **78**, 020503(R) (2008).
[16] A. I. Goldman, D. N. Argyriou, B. Ouladdiaf, T. Chatterji, A. Kreyssig, S. Nandi, N. Ni, S. L. Bud'ko, P. C. Canfield, and R. J. McQueeney, Phys. Rev. B **78**, 100506(R) (2008).
[17] Chang Liu, G. D. Samolyuk, Y. Lee, Ni Ni, Takeshi Kondo, A. F. Santander-Syro, S. L. Bud'ko, J. L. McChesney, E. Rotenberg, T. Valla, A. V. Fedorov, P. C. Canfield, B. N. Harmon, and A. Kaminski, Phys. Rev. Lett. **101**, 177005 (2008).
[18] F. Ma, Z. Lu, and T. Xiang, arXiv:0806.3526 (unpublished).
[19] R. Sknepnek, G. Samolyuk, Y.-B. Lee, and J. Schmalian, Phys. Rev. B **79**, 054511 (2009).
[20] M. A. Tanatar, A. Kreyssig, S. Nandi, N. Ni, S. L. Bud'ko, P. C. Canfield, A. I. Goldman, and R. Prozorov, Phys. Rev. B **79**, 180508(R) (2009).
[21] T.-M. Chuang, M. P. Allan, Jinho Lee, Yang Xie, Ni Ni, S. L. Bud'ko, G. S. Boebinger, P. C. Canfield, and J. C. Davis, Science **327**, 181 (2010).